AN EFFICIENT TWO-STEP PROCEDURE FOR COMPRESSED SENSING 3D MIMO RADAR

Rafael Pinto and Ricardo Merched

Dept. of Electronics and Computer Engineering
Universidade Federal do Rio de Janeiro
rafaelgcpp@gmail.com, r.merched@gmail.com

ABSTRACT

In MIMO Radar schemes, sparse scenarios have been successfully exploited by compressed sensing (CS) techniques. We address the ill-conditioning inherent to the linear model of a 3D Radar imaging system, by proposing a two-step decoupling procedure which induces structure, and allows for fast matrix products to efficiently recover the target image. This is accomplished by further combining it with an *Approximate Message Passing* algorithm, that yields two iterative versions for range and cross-range image recovery. Simulations suggest that besides computational efficiency, decoupling the full model matrix gives us more freedom in selecting the CS regularization levels. An FDTD based experiment also shows that the algorithms are robust in real life situations where non-ideal antennas and multiple scattering naturally occur.

Index Terms— MIMO Radar, Compressed Sensing

1. INTRODUCTION

In many Multi-Input-Multi-Output (MIMO) Radar scenarios, range and cross-range parameters are commonly treated separately [1],[2]. The received signals normally undergo a bank of matched filters, whose delays are set in correspondence to the desired range bins, for which the directions and reflectances of the targets are identified. In [1], e.g., this is achieved by least-squares (LS) and Capon beamformation, while [2] derives recovery conditions for compressed sensing (CS) matrices constructed by randomly located arrays.

Recently, in [3], we have approached the MIMO radar problem as a joint range/cross-range convolution model, and obtained approximate conditions for which the mutual coherence of the overall system sensing matrix is minimized. In this paper, we take a step further by decoupling the full Radar relation into two separate sparse problems, albeit ones that exhibit more structured models, suitable for efficient implementations. Although the analysis of the mutual coherence conditions for each matrix alone bears equivalence to the one obtained in the joint model, the approach here induces a level of structure that can be taken advantage from when using state-of-the-art iterative algorithms for compressed sensing, such as the *Complex Approximate Message Passing* (CAMP) algorithm studied in [4].

We present two efficient algorithms for CS radar imaging, and compare their simulated results: the first one is the iterative implementation of the joint range/cross-range formation of [3], while the second is the proposed two-step implementation. Besides efficiency, simulations indicate that the two-step version is more robust, as the regularization parameters can be adjusted separately. A *finite-difference time-domain* (FDTD) experiment is also included in order to verify the robustness of the algorithm in a more realistic scenario, with multiple scattering and non-ideal antennas.

2. JOINT RANGE/CROSSRANGE MODEL FOR MIMO RADARS

Consider the MIMO radar arrangement depicted in Fig. 1, consisting of an array of M_T isotropic transmitters, each positioned at $\mathbf{q}_m$, and a second array of M_R receivers, at positions denoted by $\tilde{\mathbf{q}}_n$. The antennas send narrowband pulses $p_i(t)$, with center frequency ω_0 through a homogeneous medium, which are scattered by K far-field targets with reflectance $\bar{s}_k$. These are located at a distance D, with directions given by unitary vectors denoted by $\bar{\mathbf{r}}_k$, which in turn are detected by the receiving array.

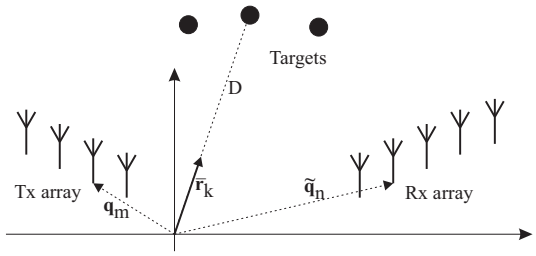

Fig. 1. Simplified schematic for a MIMO radar. All targets are located at the same range.

The manifold vectors for the transmitting array are defined as

$$\mathbf{a}(\bar{\mathbf{r}}_k) = \left[e^{j\frac{\omega_0}{c_0}\bar{\mathbf{r}}_k^T\mathbf{q}_0} \quad e^{j\frac{\omega_0}{c_0}\bar{\mathbf{r}}_k^T\mathbf{q}_1} \quad \dots \quad e^{j\frac{\omega_0}{c_0}\bar{\mathbf{r}}_k^T\mathbf{q}_{M_T-1}} \right]^T \quad (1)$$

with analogous definition for the receiving manifold vector denoted by $\mathbf{b}(\bar{\mathbf{r}}_k)$, where $c_0 \triangleq \lambda_0/2\pi\omega_0$ is the speed of propagation for the underlying medium.

978-0-9928626-3-3/15/$31.00 ©2015 IEEE

Under the well known *Born* approximation [5], the received waveform can be written as:

$$\mathbf{y}_r(t) = \sum_{k=0}^{K-1} \bar{x}_k \mathbf{b}(\bar{\mathbf{r}}_k) \left[\mathbf{p}^T(t-2\tau_r)\mathbf{a}(\bar{\mathbf{r}}_k)\right] \; + \; \mathbf{n}(t) \quad (2)$$

where the transmited pulse vector $\mathbf{p}(t)$ in (2) is denoted by $\mathbf{p}(t) \triangleq \begin{bmatrix} p_0(t) & p_1(t) & \cdots & p_{M_T-1}(t) \end{bmatrix}^T$, $\tau_r \triangleq {}^{D}/_{c_0}$, $\mathbf{n}(t)$ is an uncorrelated additive noise, and $\bar{x}_k$ is the free space path loss which we express here as a corrected reflectance for the k-th target as $\bar{x}_k \triangleq -\omega_0^2/\left(16\pi^2 c_0^2 \tau_r^2\right)\bar{s}_k = -1/\left(4\lambda_0^2\tau_r^2\right)\bar{s}_k$.

A typical radar application forms an image from the measured data; this means recovering not only the reflectances $\bar{x}_k$, but also the directions $\bar{\mathbf{r}}_k$. Frequently, those directions are obtained by beamforming techniques or by spectral DOA estimation methods, just like the MUSIC or the ESPRIT [6]. On the other hand, beamforming can be understood as probing each direction $\mathbf{r}_l$ at a fine grid defined by $G \geq K$ directions containing all targets, meaning that $\{\mathbf{r}_l | 0 \leq l \leq G\} \supseteq \{\bar{\mathbf{r}}_k | 0 \leq k \leq K\}$. In this manner, the resulting reflectance vector will be a sparse vector $\mathbf{x}_r$ with K non-zero entries, corresponding to the values of $\bar{\mathbf{x}}_r$ for which the directions $\bar{\mathbf{r}}_k$ and $\mathbf{r}_l$ coincide.

That is, sampling the received vector, i.e. $\mathbf{y}_r(n) \triangleq \mathbf{y}_r(2\tau_r + nt_s)$ and defining $\mathbf{p}(n) \triangleq \mathbf{p}(nt_s)$, we rewrite (2) as

$$\mathbf{y}_r \triangleq \begin{bmatrix} \mathbf{y}_r^T(N-1) & \mathbf{y}_r^T(N-2) & \cdots & \mathbf{y}_r^T(0) \end{bmatrix}^T \quad (3)$$

$$= \sum_{k=0}^{G-1} \left[\mathbf{P}\mathbf{a}(\mathbf{r}_k)\right] \otimes \mathbf{b}(\mathbf{r}_k) x_k \; + \; \mathbf{n}\,, \quad (4)$$

where $\otimes$ denotes the Kronecker product,

$$\mathbf{P} = \begin{bmatrix} \mathbf{p}(N-1) & \cdots & \mathbf{p}(0) \end{bmatrix}^T \quad (5)$$

is a $N \times M_T$ matrix representing the "unrolled" pulses which are N-samples long, and $\mathbf{n}$ is the corresponding sampled noise vector. Equation (3) can be equivalently written as

$$\begin{aligned} \mathbf{y}_r &= \mathbf{F}_r \mathbf{x}_r + \mathbf{n} \\ &= \begin{bmatrix} \mathbf{f}_r(\mathbf{r}_0) & \mathbf{f}_r(\mathbf{r}_1) & \cdots & \mathbf{f}_r(\mathbf{r}_{G-1}) \end{bmatrix} \mathbf{x}_r + \mathbf{n} \end{aligned} \quad (6)$$

where $\mathbf{x}_r \triangleq \begin{bmatrix} x_0 & x_1 & \cdots & x_{G-1} \end{bmatrix}^T$, and $\mathbf{F}_r$ is $NM_R \times G$, with each column given by

$$\mathbf{f}_r(\mathbf{r}_k) = \left[\mathbf{P}\mathbf{a}(\mathbf{r}_k)\right] \otimes \mathbf{b}(\mathbf{r}_k) \quad (7)$$

$$= \left[\mathbf{P} \otimes \mathbf{I}_{M_R}\right] \left[\mathbf{a}(\mathbf{r}_k) \otimes \mathbf{b}(\mathbf{r}_k)\right] \; . \quad (8)$$

Note that $\mathbf{F}_r$ is rank deficient, with $\mathrm{rank}(\mathbf{F}_r) \leq M_T M_R$. Now, defining $\mathbf{c}_k = \mathbf{a}(\mathbf{r}_k) \otimes \mathbf{b}(\mathbf{r}_k)$, we can express (6) as

$$\mathbf{y}_r = \left[\mathbf{P} \otimes \mathbf{I}_{M_R}\right] \mathbf{C}\, \mathbf{x}_r + \mathbf{n} \quad (9)$$

where $\mathbf{C} \triangleq \begin{bmatrix} \mathbf{c}_0 & \mathbf{c}_1 & \cdots & \mathbf{c}_{G-1} \end{bmatrix}$, represents the $M_T M_R \times G$ combined manifold matrix.

Moreover, extending this model to multiple ranges, $\mathbf{x}_r$ becomes a function of the range delay τ_r, so that the received signal must be replaced by a convolution integral:

$$\mathbf{y}(t) = \int \sum_{k=0}^{G-1} x_k(\tau_r) \mathbf{b}(\mathbf{r}_k) \left[\mathbf{p}^T(t-2\tau_r)\mathbf{a}(\mathbf{r}_k)\right] \mathrm{d}\tau_r + \mathbf{n}(t) \quad (10)$$

In this case, sampling $\mathbf{y}(t)$ at nt_s, and defining $\tau_n \triangleq \tau_0 - nt_s/2$, assuming that all targets are confined to Q range bins, we can rewrite (10) blockwise as $\mathbf{y} = \mathcal{F}\mathbf{x}$, where $\mathcal{F}$ has a $M_R(N+Q-1) \times QG$ block-Toeplitz structure, which for convenience we partition into its respective block columns:

$$\mathcal{F} = \begin{bmatrix} \mathcal{F}_0 & \mathcal{F}_1 & \cdots & \mathcal{F}_{Q-1} \end{bmatrix}. \quad (11)$$

The vector $\mathbf{x}$ is composed by stacking the reflectance vectors $\mathbf{x}_r$ for all ranges. Each $\mathcal{F}_n$ has now the same structure of $\mathbf{F}_r$, whose columns are obtained by replacing the columns of $\mathbf{P}$ in Eq. (8) with their respective zero-padded versions, say, $\mathcal{P}_n \triangleq \begin{bmatrix} \mathbf{0}_{M_T \times n} & \mathbf{P}^T & \mathbf{0}_{M_T \times (Q-1)-n} \end{bmatrix}^T$.

Alternatively, introduce $\mathbf{S} \triangleq \begin{bmatrix} \mathcal{P}_0 & \mathcal{P}_1 & \cdots & \mathcal{P}_{Q-1} \end{bmatrix} \otimes \mathbf{I}_{M_R}$ and $\mathcal{C} \triangleq \mathrm{diag}\left\{ \mathbf{C} \cdots \mathbf{C} \right\} = \mathbf{I}_Q \otimes \mathbf{C}$. This yields

$$\mathbf{y} = \mathbf{S}\mathcal{C}\,\mathbf{x} = \mathbf{S}\,\mathrm{vec}(\mathbf{C}\mathbf{X}), \quad (12)$$

where $\mathbf{X}$ is the reshaped vector $\mathbf{x}$ into a size $G \times Q$ matrix. Equation (12) also makes evident that $\mathcal{F}$ is rank deficient, again, with $\mathrm{rank}(\mathcal{F}) \leq M_T M_R$.

Recovering the support of the vector $\mathbf{x}$ in this model determines the directions of arrival and the range bins containing the desired targets. As the measurement matrix is rank deficient, LS or MMSE estimation methods fail to recover the correct solution. Usually, the target vector is sparse, suggesting that we can resort to compressed sensing techniques so as to overcome this limitation.

3. MANIFOLD MATRIX AS A COMPRESSIVE FRAME

One traditional array geometry is the uniform linear array (ULA), composed by M equally spaced elements, which can be aligned with the z-axis; the coordinates of each sensor in this case can be represented as $\mathbf{q}_i = \begin{bmatrix} 0 & 0 & id + q_0 \end{bmatrix}^T$, where d is the spacing between its elements and q_0 is the position of the first array element on the z-axis. Since the direction of arrival vector depends on a single angle, say, ϕ_k, the transmitter manifold vector (1) can be equivalently written as

$$\mathbf{a}(\psi_k) = e^{jq_0\psi_k} \begin{bmatrix} 1 & e^{jd_T\psi_k} & \cdots & e^{j(M_T-1)d_T\psi_k} \end{bmatrix}^T, \quad (13)$$

where $\psi_k \triangleq (\omega_0/c_0)\sin\phi_k$, and d_T is the spacing between transmitting elements. Again, we have an analogous definition for the receiver manifold vector $\mathbf{b}(\psi_k)$, comprising d_R spaced elements, with first element at $\tilde{q}_0$. If we set $d_T = M_R d_R$, then each vector $\mathbf{c}_k$ can be viewed as an equivalent manifold vector having $M \triangleq M_T M_R$ entries, with spacing $d = d_R$ and first element at $z_0 \triangleq q_0 + \tilde{q}_0$. Such arrangement is commonly known as a *virtual* ULA [7]. For convenience, we write $\mathbf{C}$ in (12) as $\mathbf{C} \triangleq \mathbf{C}_V \mathbf{D}$, where $\mathbf{D} = \mathrm{diag}\left\{ e^{jz_0\psi_0} \quad e^{jz_0\psi_1} \quad \cdots \quad e^{jz_0\psi_{(G-1)}} \right\}$, and $\mathbf{C}_V$ is an $M \times G$ matrix of discrete Fourier bases defined by the node vector $\begin{bmatrix} e^{jd\psi_0} & e^{jd\psi_1} & \cdots & e^{jd\psi_{G-1}} \end{bmatrix}$.

Now, from (12), let

$$\mathbf{z} \triangleq \mathrm{vec}(\mathbf{C}\mathbf{X}) \quad (14)$$

so that $$\mathbf{y} = \mathbf{S}\,\mathbf{z}\,. \tag{15}$$

It is known that $M \times G$ Fourier matrices composed by distinct bases are full spark, with equal norm columns, given that $M \leq G$ (see [8]). Moreover, it is also known that if $\mathbf{C}$ is full spark, this condition allows us to robustly recover the columns of $\mathbf{X}$ that are up to $G/2$-sparse, given that we can recover $\mathbf{z}$ from $\mathbf{y}$. Fourier matrices with equally spaced bases in the unit circle can be shown to satisfy the *Restricted Isometry Property* (RIP), and exhibit the smallest worst-case coherence when $G \geq 2M$ [8]. We can take advantage of such fact by choosing the probing directions in (13) as $\psi_k \triangleq \psi_0 + k\delta$, with $0 < k < G$. As a result, it can be easily verified that $\mathbf{C} = e^{jz_0\psi_0}\mathbf{D}_1\mathbf{C}_F\mathbf{D}_2$, where $\mathbf{D}_1 = \operatorname{diag}\left\{1 \quad e^{jd\psi_0} \quad \cdots \quad e^{j(M-1)d\psi_0}\right\}$, $\mathbf{D}_2 = \operatorname{diag}\left\{1 \quad e^{jz_0\delta} \quad \cdots \quad e^{jz_0(G-1)\delta}\right\}$, and $\mathbf{C}_F$ is an $M \times G$ partial DFT matrix with $e^{jd\delta}$ as basis.

In most practical scenarios, when $\mathbf{C}$ is essencially a partial DFT matrix, $\mathbf{z}$ will be quasi-sparse: if a column of the target image $\mathbf{X}$ contains a wide target, its corresponding column in $\mathbf{Z} \triangleq \mathbf{C}\mathbf{X}$ will exhibit localized elements (Fourier bandwidth trade-off). Thus, the only situation where we would have a dense matrix $\mathbf{Z}$ is when $\mathbf{X}$ represents a very narrow (cross-range) and long (range) target.

Henceforth, assuming $\mathbf{z}$ to be sparse, it can be fully recovered using compressed sensing techniques from $\mathbf{y}$ by designing the columnns of $\mathbf{S}$ to have low mutual coherence, which is defined as [9]:

$$\mu(\mathbf{S}) = \max_{i \neq j} \frac{|[\mathbf{S}]_i^*[\mathbf{S}]_j|}{\|[\mathbf{S}]_i\|_2 \|[\mathbf{S}]_j\|_2}, \tag{16}$$

where $[\mathbf{S}]_j$ denotes the j-th column of $\mathbf{S}$, and * the complex transposition. Now, to compute the mutual coherence one can take advantage of the structure in $\mathbf{S}$, whose Gram matrix turns up block-Toeplitz. In this case, each such block is given by

$$\mathbf{G}(l-m) = [\mathcal{P}_l \otimes \mathbf{I}_{M_R}]^* [\mathcal{P}_m \otimes \mathbf{I}_{M_R}] \tag{17}$$

$$= \mathbf{R}(l-m) \otimes \mathbf{I}_{M_R}, \tag{18}$$

where $\mathbf{R}(l-m) \triangleq \mathcal{P}_l^*\mathcal{P}_m$ is the pulse vector autocorrelation function. Assuming that all pulses have the same power, then the diagonal elements of $\mathbf{G}(0)$ become constant, and we can optimize $\mu(\mathbf{S})$ by minimizing all off-diagonal elements of the Gram matrix. This can be achieved by approximating $\mathbf{R}(0) = N\mathbf{I}_{M_T}$ and $\mathbf{R}(k) = \mathbf{0}, 0 < k < Q$. Independent Gaussian sequences sets, as considered in [10], allows us to approximate these requirements in a stochastic way. As an alternative, we make use of the so-called *complementary sequences sets*, which can be generated by optimizing the following block LS criterion (see Eq. (11) in [1]):

$$\min_{\mathbf{R}(k)} \|\mathbf{R}(0) - N\mathbf{I}\|_F^2 + 2\sum_{k=1}^{Q-1} \|\mathbf{R}(k)\|_F^2 \tag{19}$$

Complementary sequences have the advantage of producing near zero correlations in a range of only $Q-1$ samples, yielding lower cross-correlations within the same range when compared to its Gaussian sequences counterpart. It is also possible to restrict the pulse samples to specific modulations, such as QAM or BPSK.

Thus, the conditions on $\mathbf{R}(k)$ are similar to those found for joint range and cross-range recovery in [3]. Additionally, if $\mathbf{C}$ is a discrete Fourier matrix with equally spaced bases, we have the appropriate conditions to attain the lower bound for the mutual coherence of $\mathcal{F}$ derived in that paper, which assumes direct recovery of $\mathbf{x}$ from $\mathbf{y}$. The advantage of recovering range and cross-range sequentially as in (14)-(15) is the freedom in controlling the regularization parameters in the CS problems for each direction individually, allowing for different levels of sparsity in $\mathbf{z}$ and $\mathbf{x}$.

4. EFFICIENT IMPLEMENTATION

Sparse recovery in compressed sensing usually reduces to ℓ_1 norm minimization via the LASSO [11] algorithm, which, for complex-valued problems, can be solved by quadratic constrained quadratic programming (QCQP). Many interior point solvers are readily available for these problems. However, such solvers are not very efficient, since for each grid point to be recovered, a significant number of constraints is added, resulting in $3QG$ variables. Furthermore, they do not take full advantage of the problem structure, as they often require the measurement matrix to be formed explicitly, and demand a QR decomposition of the *Karush-Kuhn-Tucker* (KKT) system at each step [11].

On the other hand, iterative algorithms like *Approximate Message Passing* (AMP) [12] and its complex domain counterpart, say, CAMP [4], are readily available for sparse recovery. The complexity of those algorithms is governed by products with the measurement matrix, which can be implemented very efficiently through (14) and (15). Here, we are assuming that the complexity of a matrix-vector product is roughly the same for the direct and transposed matrix operations.

Unlike the direct product $\mathcal{C}\mathbf{x}$, which in general requires GM_TM_RQ operations, the block diagonal products require only $Q[G\log_2 G + G + M_TM_R]$ operations if $\mathbf{C}$ is a Fourier matrix. Recognizing the block-Toeplitz like structure in $\mathbf{S}$ we can reduce the operations count for $\mathbf{S}\mathbf{z}$ from $M_R^2M_TNQ$ to $(N+Q-1)M_T[M_TM_R + (M_R+2)\log_2(N+Q-1)]$, by using FFT based algorithms.

For the sake of comparison, we implement two iterative procedures. The first one is a CAMP-based implementation of [3], where we recover $\mathbf{x}$ directly from $\mathbf{y}$. In this version, each algorithm iteration requires the computation of $\mathbf{S}\mathcal{C}\mathbf{x}$ and $\mathcal{C}^*\mathbf{S}^*\mathbf{y}$. In the second version, we considered the two-step procedure aforementioned, first recovering $\mathbf{z}$ from $\mathbf{y}$ (which makes use of products like $\mathbf{S}\mathbf{z}$ and $\mathbf{S}^*\mathbf{y}$). Having recovered $\mathbf{z}$, we reshape it and use CAMP for each column of $\mathbf{Z}$, say, $[\mathbf{Z}]_i$, so as to retrieve the columns of $\mathbf{X}$. In this step, the products used are mainly $\mathbf{C}[\mathbf{X}]_i$ and $\mathbf{C}^*[\mathbf{Z}]_i$.

Note that the two algorithm versions will exhibit the same worst case complexity, if we consider that CAMP will always require the same maximum number of iterations to converge. In practice, the second version is marginally faster, as CAMP converges in a smaller number of iterations in the second step, where the problems are smaller.

5. EXPERIMENTS

Figure 2 shows the exact target image considered in all experiments. The simulated system employs $M_T = 7$ transmitters and $M_R = 10$ receivers, in a virtual ULA configuration. The transmitted (complementary) sequences were generated by the WeCAN algorithm proposed in [1] of length $N = 256$ and a zero cross-correlation zone covering $Q = 48$ samples.

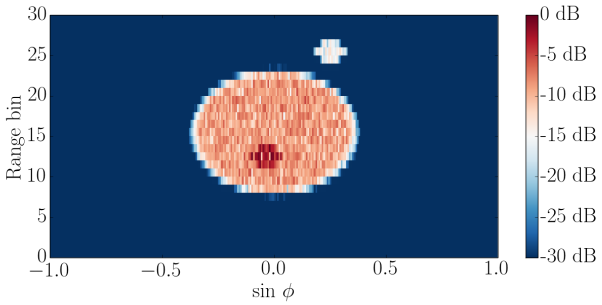

Fig. 2. True target image.

All experiments were performed under 20 dB and 5 dB signal-to-noise-ratio (SNR). As a basis of comparison, Fig. 3 shows the recovery using matched filters for LS beamforming, traditionally used for imaging systems, similar to the experiment in [1]. Although the main part of the target is recovered, the detached piece with lower reflection coefficient is obscured by the interference pattern, even in high SNR.

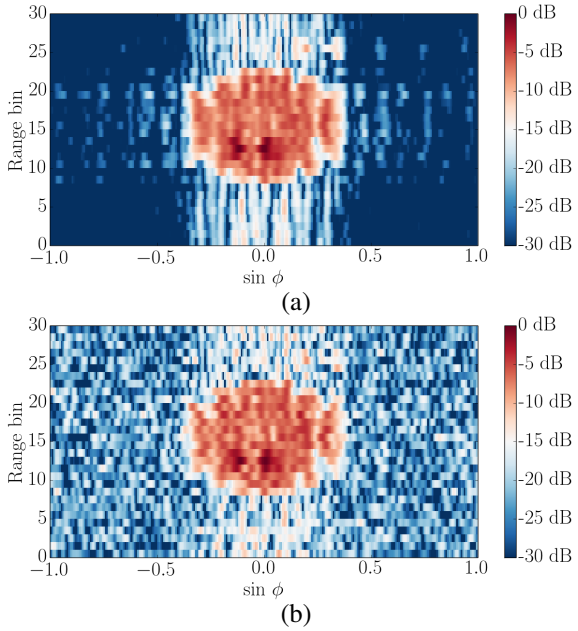

Fig. 3. LS recovery at (a) 20 dB SNR and (b) 5 dB SNR.

Figures 4 (a) and (b) show the result for recovering the image in a single CAMP step, as in [3]. The use of compressed sensing techniques for joint range and cross-range imaging greatly improves the reconstruction, even in low SNR.

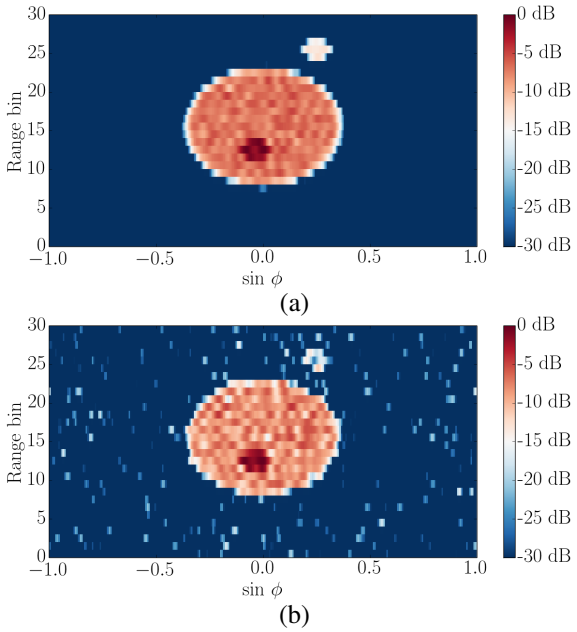

Fig. 4. Joint range and cross-range recovery [3] at (a) 20 dB SNR and (b) 5 dB SNR.

The second algorithm, which forms the image in two steps, is shown in Figs. 5 (a) and (b). The resolved image is very similar to the single step version, but the detached element is more clearly identified in the low SNR scenario. Also, the noise speckles around the main target are less prominent, due to different regularization levels applied in each step.

The last experiment is an FDTD simulated scene containing two small solid boxes with different uniform dielectric constants and a small electrical conductivity, and is intended to verify the algorithm behavior under some more realistic conditions such as non-ideal antenna patterns and multiple scattered signals. Figure 6 shows the result, again for three different recovery algorithms. For this simulation, we make use of the OpenEMS package [13], with $M_T = 5$ transmitting elements and $M_R = 11$ receiving antennas. Since electromagnetic waves are reflected solely at media interfaces, only the borders within the critical angle become visible, as it would happen to a glass cube. The higher reflectances correspond to the box corners, and the apparent angular distortion seen is an effect of the non-cartesian mapping of the axes [The expected recovered shape of the boxes is shown in the insertion at the bottom of Fig. 6 (a)-(c)]. Again, the two-step algorithm results in the best image. In between the boxes it appears the effect of re-scattered fields, not taken into account by the Born approximation used in first place.

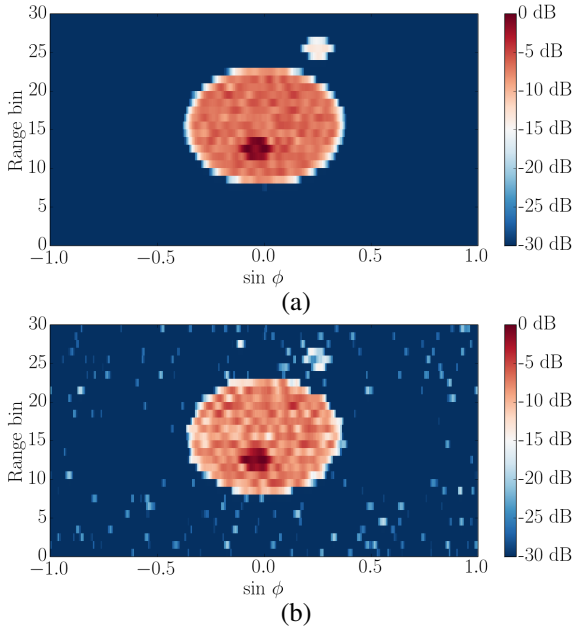

Fig. 5. Two-step range and cross-range recovery at (a) 20 dB SNR and (b) 5 dB SNR.

6. CONCLUDING REMARKS

In this paper, we have proposed efficient algorithms for image reconstruction in a full 3D compressed sensing MIMO radar scenario. Under an additive noise model, the two-step version allows for better control on the regularization parameters, improving the reconstruction. The FDTD simulation corroborates with the results, showing an adequate recovery even with non-ideal antennas and multi-scattered signals.

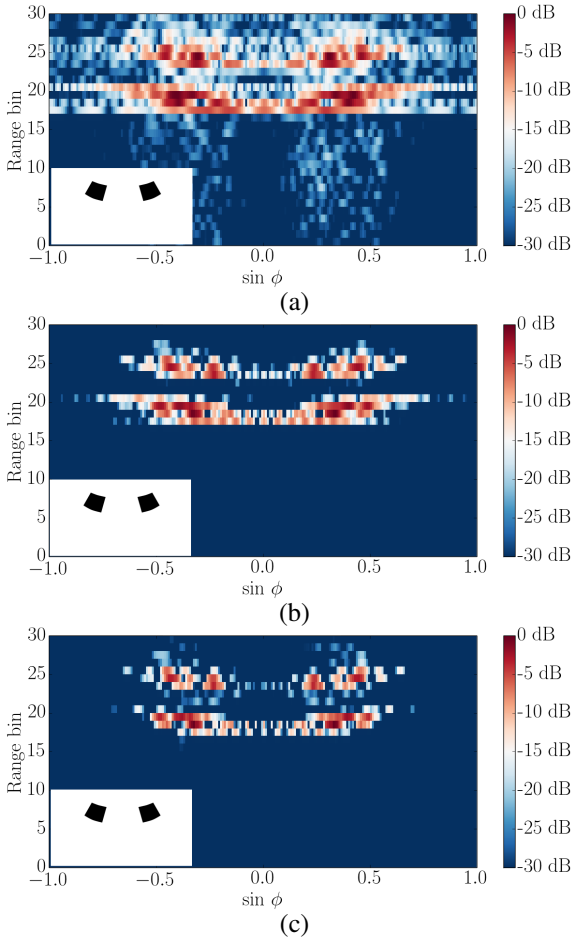

Fig. 6. FDTD image using (a) LS recovery and (b) single-step and (c) two-step joint range and crossrange recovery.

REFERENCES

[1] H. He, P. Stoica, and J. Li, "Designing unimodular sequence sets with good correlations - including an application to MIMO radar," *IEEE Trans. on Sig. Proc.*, vol. 57, no. 11, pp. 4391–4405, Nov 2009.

[2] M. Rossi, A.M. Haimovich, and Y.C. Eldar, "Spatial compressive sensing for MIMO radar," *IEEE Trans. on Sig. Proc.*, vol. 62, no. 2, pp. 419–430, Jan 2014.

[3] R. G. Pinto and R. Merched, "Compressed sensing joint range and cross-range MIMO radar imaging," in *Proc. of IEEE ICASSP 2015, to appear*, 2015.

[4] A. Maleki, L. Anitori, Z. Yang, and R.G. Baraniuk, "Asymptotic analysis of complex lasso via complex approximate message passing (CAMP)," *IEEE Trans. on Inf. Theory*, vol. 59, no. 7, pp. 4290–4308, July 2013.

[5] M. Cheney, "A mathematical tutorial on synthetic aperture radar," *SIAM Rev.*, vol. 43, pp. 301–312, Feb. 2001.

[6] H. L. Van Trees, *Optimum Array Processing (Detection, Estimation, and Modulation Theory, Part IV)*, Wiley-Interscience, 1 edition, Mar. 2002.

[7] J. Li, P. Stoica, L. Xu, and W. Roberts, "On parameter identifiability of MIMO radar," *IEEE Sig. Proc. Letters*, vol. 14, no. 12, pp. 968–971, 2007.

[8] B. Alexeev, J. Cahill, and D.G. Mixon, "Full spark frames," *Journal of Fourier Anal. and App.*, vol. 18, no. 6, pp. 1167–1194, 2012.

[9] Y. C. Eldar and G. Kutyniok, Eds., *Compressed Sensing: Theory and Applications*, Cambridge University Press, 2012.

[10] T. Strohmer and B. Friedlander, "Analysis of sparse MIMO radar," *CoRR*, vol. abs/1203.2690, 2012.

[11] S. Boyd and L. Vandenberghe, *Convex Optimization*, Cambridge University Press, New York, NY, USA, 2004.

[12] D. L. Donoho, A. Maleki, and A. Montanari, "Message-passing algorithms for compressed sensing," *Proc. of the Nat. Acad. of Sci.*, vol. 106, no. 45, pp. 18914–18919, 2009.

[13] T. Liebig, A. Rennings, S. Held, and D. Erni, "OpenEMS-a free and open source equivalent-circuit (EC) FDTD simulation platform supporting cylindrical coordinates suitable for the analysis of traveling wave MRI applications," *Intl. Journal of Num. Modelling: Elec. Networks, Dev. and Fields*, vol. 26, no. 6, pp. 680–696, 2013.